

Chondrule Destruction via Dust Collisions in Shock Waves

YUJI MATSUMOTO,¹ KOSUKE KUROSAWA,^{2,3} AND SOTA ARAKAWA⁴

¹*National Astronomical Observatory of Japan, 2-21-1, Osawa, Mitaka, 181-8588 Tokyo, Japan*

²*Department of Human Environmental Science, Graduate school of Human Development and Environment, Kobe University, 3-11, Tsurukabuto, Nada-ku, Kobe, Hyogo 657-8501, Japan*

³*Planetary Exploration Research Center, Chiba Institute of Technology, 2-17-1, Narashino, Tsudanuma, Chiba 275-0016, Japan*

⁴*Japan Agency for Marine-Earth Science and Technology, 3173-25, Showa-machi, Kanazawa-ku, Yokohama, Kanagawa 236-0001, Japan*

ABSTRACT

A leading candidate for the heating source of chondrules and igneous rims is shock waves. This mechanism generates high relative velocities between chondrules and dust particles. We have investigated the possibility of the chondrule destruction in collisions with dust particles behind a shock wave using a semianalytical treatment. We find that the chondrules are destroyed during melting in collisions. We derive the conditions for the destruction of chondrules and show that the typical size of the observed chondrules satisfies the condition. We suggest that the chondrule formation and rim accretion are different events if they are heated by shock waves.

Keywords: Chondrules(229) — Chondrites(228)

1. INTRODUCTION

Chondrules are spherical-shaped igneous grains in chondrites. They were once wholly or partially molten by flash heating events in the solar nebula (e.g., [Hewins et al. 2005](#)). Chondrules are the most abundant ingredients of most chondrites, suggesting that flash heating events in the solar nebula were frequent. The heating processes of chondrules are still under debate. Several heating mechanisms have been proposed so far, including shock waves (e.g., [Hood & Horanyi 1991](#); [Miura & Nakamoto 2005](#)), planetesimal collisions (e.g., [Asphaug et al. 2011](#); [Johnson et al. 2015](#); [Wakita et al. 2017](#)), and lightning (e.g., [Horányi et al. 1995](#); [Kaneko et al. 2023](#)).

Rims are the surrounding structures of chondrules. There are two major categories pertaining to rims: fine-grained rims and igneous rims. Fine-grained rims are composed of matrix-like dust grains (e.g., [Ashworth 1977](#); [Huss et al. 2005](#)). The origin of the fine-grained rims is mainly interpreted as the accretion of dust particles onto the surfaces of chondrules (e.g., [Metzler et al. 1992](#); [Matsumoto et al. 2019](#); [Kaneko et al. 2022](#)). Igneous rims are composed of coarse-grained dust particles and show evidence of a high degree of melting

(e.g., [Rubin 1984](#); [Krot & Wasson 1995](#)). The dust particles in the igneous rim components underwent flash heating events similar to those that formed the chondrule. Igneous rims would be formed by melting of accretionary rims (e.g., [Rubin 1984, 2010](#)) and the accretion of droplets ([Kring 1991](#); [Jacquet et al. 2013](#); [Matsumoto et al. 2021](#); [Matsumoto & Arakawa 2023](#)).

The presence of the rims suggests that chondrules and dust particles coexisted in the solar nebula. Chondrules accrete dust particles during or after heating events. The accretion conditions of the chondrule-dust collisions depend on the impact velocity and their physical states. In particular, chondrules are expected to be destroyed if the impact velocity is too high.

Previous studies have pointed out the possibility of chondrule destruction in shock heating events. In this flash heating process, chondrules are decelerated by the gas drag force in the post-shock regions (e.g., [Hood & Horanyi 1991](#); [Iida et al. 2001](#)). Dust particles of different sizes have relative velocities due to the size dependence of the stopping time. [Nakamoto & Miura \(2004\)](#) evaluated the collisional destruction rate of chondrules adopting the destruction criterion based on the impact fragmentation experiment ([Takagi et al. 1984](#)). They showed that chondrules larger than a critical radius are destroyed. [Jacquet & Thompson \(2014\)](#) pointed out that impact fragmentation debris promotes the destruc-

tion of chondrules. Ciesla (2006) considered collisions between molten chondrules. Molten chondrules have different criteria for adhesion and destruction from the chondrules after crystallization. Ciesla (2006) estimated the impact velocity for the destruction of molten chondrules with viscosities of 100 poise (P) and showed that the molten chondrules are destroyed when the impact velocity is higher than $\sim 100 \text{ m s}^{-1}$. They also showed that chondrules can avoid destructive collisions during melting because only a small number of chondrules collide during melting.

Here we have revisited the possibility of the collisional disruption of chondrules behind a shock wave. We propose a new scenario for the collisional disruption of chondrules (or chondrule precursors): the destruction of molten chondrules by collisions with $\sim 10 \mu\text{m}$ dust particles. Our results suggest that the chondrule-forming shock events occur in $\sim 10 \mu\text{m}$ dust-free environments, while the rim-accreting shock events occur in the presence of $\sim 10 \mu\text{m}$ dust particles. The plan of our paper is as follows. We describe our model in Section 2. We show the typical evolution of chondrules and the parameter dependence in Section 3. Our conclusion and discussion is given in Section 4, where we discuss the conditions of the chondrule-forming shock and the rim-accreting shock.

2. MODEL

Chondrules (precursors) and dust particles are decelerated and heated behind the shock front. A chondrule collides with dust particles according to the number density of the dust, the collisional cross section, and their relative velocities. We adopt the one-dimensional normal shock model used in Matsumoto & Arakawa (2023) to consider the destruction of chondrules in collisions.

2.1. Gas Structure

A simple gas structure is assumed according to previous studies (e.g., Nakamoto & Miura 2004; Ciesla 2006; Jacquet & Thompson 2014; Arakawa & Nakamoto 2019; Matsumoto & Arakawa 2023). Here, we briefly describe the key equations with the numbers used in the model. The details can be found in the original studies. The gas velocity with respect to the shock front, v_g , is given by

$$v_g = \begin{cases} v_0 & (x < 0), \\ v_0 + (v_{\text{post}} - v_0) \exp(-x/L) & (x \geq 0), \end{cases} \quad (1)$$

where v_0 is the gas velocity with respect to the shock front in the preshock region, namely, shock velocity, v_{post} is the postshock gas velocity with respect to the shock front, $L = 10^3 \text{ km}$ (Miura & Nakamoto 2005)

is the spatial scale of the shock, and x is the distance from the shock front. The postshock gas velocity is given by the Rankine–Hugoniot relations, $v_{\text{post}} = [(\gamma - 1)/(\gamma + 1)]v_0$, where the ratio of specific heat is $\gamma = 1.4$ for the nebula gas composed of molecular hydrogen. The gas temperature is

$$T_g = \begin{cases} T_0 & (x < 0), \\ T_0 + (T_{\text{post}} - T_0) \exp(-x/L) & (x \geq 0), \end{cases} \quad (2)$$

where the preshock temperature is $T_0 = 500 \text{ K}$ and the postshock gas temperature is $T_{\text{post}} = 2000 \text{ K}$ (Miura et al. 2002). According to the Rankine–Hugoniot and isobaric relations, the gas number density can be expressed as

$$n_g = n_0 \frac{T_0}{T_g} \frac{4s_0^2 - (\gamma - 1)}{\gamma + 1}, \quad (3)$$

where $n_0 = 10^{14} \text{ cm}^{-3}$ is the preshock gas number density, $s_0 = v_0/(2k_{\text{B}}T_0/m_g)^{1/2}$, k_{B} is the Boltzmann constant, and $m_g = 3.34 \times 10^{-24} \text{ g}$ is the mass of H_2 .

2.2. Dynamical and Temperature Evolution of Chondrules and Dust

Chondrules and dust particles are decelerated once and then accelerated by interaction with the gas behind the shock front. Their velocities with respect to the shock front are given by

$$m \frac{dv}{dx} = -\frac{C_D}{2} \pi a^2 m_g n_g \frac{|v - v_g|}{v} (v - v_g), \quad (4)$$

where v , m , and a are the velocity, mass, and radius of a chondrule (ch) or dust particle (d), respectively. The radii of the chondrules are our parameters and $a_d = 20 \mu\text{m}$. The density of the chondrules and dust particles are $\rho = 3.3 \text{ g cm}^{-3}$ (e.g., Friedrich et al. 2015). The drag coefficient, C_D , is given by (Hood & Horanyi 1991)

$$C_D \simeq \frac{2\sqrt{\pi}}{3s} + \frac{2s^2 + 1}{\sqrt{\pi}s^3} \exp(-s^2) + \frac{4s^4 + 2s^2 - 1}{2s^4} \text{erf}(s). \quad (5)$$

where $s = v/(2k_{\text{B}}T_g/m_g)^{1/2}$. The stopping length of a particle becomes

$$l_{\text{stop}} \equiv \left(\frac{1}{v} \frac{dv}{dx} \right)^{-1} \simeq 1.3 \times 10^2 \text{ km} \left(\frac{a}{100 \mu\text{m}} \right) \left(\frac{n_0}{10^{14} \text{ cm}^{-3}} \right)^{-1} \times \left(\frac{v_0}{10 \text{ km s}^{-1}} \right)^{-2} \left(\frac{v}{v - v_g} \right)^2. \quad (6)$$

The temperature evolution of a particle is given by the equation of energy,

$$m c_{\text{heat}} \frac{dT}{dx} = \frac{4\pi a^2}{v} (\Gamma - \Lambda_{\text{rad}} - \Lambda_{\text{evap}}), \quad (7)$$

where $c_{\text{heat}} = 1.42 \times 10^7 \text{ erg g}^{-1} \text{ K}^{-1}$ is the specific heat, which is taken from the value of forsterite¹ (Miura et al. 2002, based on NIST WebBook), Γ is the heating rate via the energy transfer from the gas, Λ_{rad} is radiative cooling, and Λ_{evap} is latent heat cooling by evaporation per unit area, respectively. The detailed expressions of Γ , Λ_{rad} , and Λ_{evap} are described in Appendix A. This equation indicates that smaller dust particles heat up more quickly.

Dust particles melt when their temperature reaches the melting temperature, $T_{\text{melt}} = 2171 \text{ K}$ (Miura et al. 2002). We consider a thermal buffering by the latent heat from solid to liquid pertaining to both chondrules and dust particles with the mass fraction of solid, S ,

$$m L_{\text{melt}} \frac{dS}{dx} = \frac{4\pi a^2}{v} (\Gamma - \Lambda_{\text{rad}} - \Lambda_{\text{evap}}), \quad (8)$$

where $L_{\text{melt}} = 4.47 \times 10^9 \text{ erg g}^{-1}$ is the latent heat of melting (Miura et al. 2002). During the phase transition ($0 < S < 1$), we assume that the temperature of a particle remains constant. We assume that the crystallization temperature of droplets is $T_c = 1000 \text{ K}$ due to supercooling².

We consider the size evolution of dust particles due to boiling and evaporation. The details are described in Appendix B. The mass density of dust particles decreases as the size of a dust particle decreases. Instead, we calculate the number density of dust particles. The number density of dust particles (n_d) is calculated from the dust-to-gas ratio in the preshock region (χ) and the continuity equation in the steady state.

2.3. Chondrule destruction

The destruction of chondrules in collisions is modeled based on impact excavation using experimental results

¹ We note that actual chondrules are not composed entirely of forsterite (e.g., Scott 2007).

² According to experimental studies (e.g., Nagashima et al. 2008), we consider that molten chondrules (precursors) turn into supercooled droplets. The supercooled droplets crystallize at the crystallization temperature, which we take from the glass transition temperature ($\approx 900\text{--}1000 \text{ K}$, e.g., Villeneuve et al. 2015). The actual crystallization temperature depends on the composition and the cooling rate. The glass transition temperature would be a lower limit of the crystallization temperature (see also Arakawa & Nakamoto 2016). The crystallization temperature does not significantly affect the results.

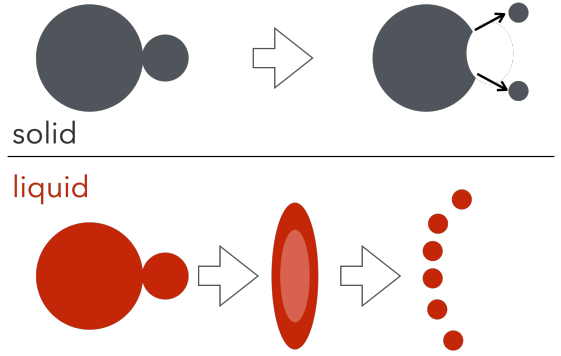


Figure 1. Schematics of the collision outcome models for the chondrules in this study. A solid chondrule is excavated by the collisions of dust particles (e.g., Suzuki et al. 2012). The droplet chondrule is destroyed by the collisions of dust particles as follows: The droplet chondrule deforms, once becomes a lamella, and is broken into secondary droplets (e.g., Pan et al. 2009).

on the crater scaling law,

$$\pi_V = 0.11 \pi_3^{-0.71} \pi_4^{0.23}, \quad (9)$$

where π_V is the dimensionless volume, π_3 is the ratio of the strength to dynamic ram pressure, and π_4 is the density ratio (e.g., Holsapple & Schmidt 1982; Holsapple 1993; Suzuki et al. 2012),

$$\pi_V = \frac{\rho_t V}{m_p}, \quad \pi_3 = \frac{Y}{\rho_p v_{\text{imp}}^2}, \quad \pi_4 = \frac{\rho_t}{\rho_p}. \quad (10)$$

The quantities with t and p are those of the target and projectile, V is the crater volume, Y is the target strength, and v_{imp} is the impact velocity. The strength of the solid chondrule is $Y_{\text{sol}} = 10 \text{ MPa}$, according to the crushing strength of the chondrule from Allende and Saratov chondrites (Wada et al. 2018). The mass-loss in a single impact excavation can be expressed as

$$\begin{aligned} m_{\text{loss}} &= \pi_V m_d \\ &\simeq 6.75 m_d \\ &\times \left(\frac{Y_{\text{sol}}}{10 \text{ MPa}} \right)^{-0.71} \left(\frac{\rho_d}{3.3 \text{ g cm}^{-3}} \right)^{0.71} \left(\frac{v_{\text{imp}}}{1 \text{ km s}^{-1}} \right)^{1.42}. \end{aligned} \quad (11)$$

We calculate the mass-loss rates of chondrules by

$$\frac{dm_{\text{ch}}}{dx} = m_{\text{loss}} n_{\text{col}} = m_{\text{loss}} n_d \pi a_{\text{ch}}^2 \frac{v_{\text{imp}}}{v_{\text{ch}}}, \quad (12)$$

for solid chondrules. Here, $n_{\text{col}} = n_d \pi a_{\text{ch}}^2 v_{\text{imp}} / v_{\text{ch}}$ is the number of collisions per unit travel length of chondrules.

We use the same model for the droplet chondrule, assuming $Y_{\text{liq}} = 0$. This assumption means that the collisions between a droplet chondrule and a droplet dust

particle cause the catastrophic destruction of the droplet chondrule (see Appendix C for the breakup criteria of collisions between droplets). Figure 1 is a schematic summary of our collision model. We calculate the cumulative number of the collisions during $S < 1$, N_S . All droplet chondrules ($S = 0$) are destroyed when $N_S = 1$ and we stop the simulation. Large chondrules cause collisions during the phase transition. During the phase transition, we remove the mass of the molten part ($(1 - S)m_{\text{ch}}$) from the chondrules when N_S reaches one, and we reset S to 1³. We neglect the effect of the impact debris (Jacquet & Thompson 2014). This is because we focus on the destruction of the chondrules during melting.

3. RESULTS

3.1. Typical Evolution

Figure 2 shows the typical evolution of chondrules and dust particles behind the shock front in the case where $v_0 = 13 \text{ km s}^{-1}$, $\chi = 0.1$, and $a_{\text{d,init}} = 20 \text{ }\mu\text{m}$. We show the evolution of the chondrules with three different sizes. In the case of the smallest chondrules ($a_{\text{ch,init}} = 10^{1.6} \text{ }\mu\text{m}$), the chondrules heat up quickly and become droplets ($S = 0$) at $x \simeq 2 \text{ km}$. The temperature of the chondrules decreases due to cooling by radiation and evaporation after they reach the peak temperature. The chondrules turn into supercooled droplets at $x = x_s \simeq 16 \text{ km}$ and crystallize at $x = x_c \simeq 1.1 \times 10^3 \text{ km} \simeq L$. The velocities of the chondrules are also quickly damped, and the relative velocity between the chondrules and dust reaches a maximum at $x = 16 \text{ km}$, which is around the stopping length of the dust particles. The maximum relative velocity is 4.7 km s^{-1} . Then, the relative velocity becomes lower as the velocities of the chondrules are damped (see Matsumoto & Arakawa 2023, for more details on the evolution of the relative velocity). The cumulative number of the collisions is $N_{\text{col,cum}} \simeq 1.8 \times 10^{-2}$ at $x = x_s$ and $N_{\text{col,cum}} \simeq 0.20$ at $x = x_c$. This indicates that about 80% of the chondrules do not experience collisions during melting and most collisions between the chondrules and dust particles occur during supercooling.

After crystallization, the chondrules are not eroded by collisions. This is because the relative velocities between the chondrules and the dust particles are very low,

and there are also no collisions. The chondrules have shorter stopping lengths than the spatial scale of the shock ($l_{\text{stop,ch}} < L$), which makes relative velocities low at $x > x_c$ ($v_{\text{rel}} < 0.07 \text{ km s}^{-1}$). The cumulative number of the collisions is $N_{\text{col,cum}} \simeq 0.21$ at $x = 10^4 \text{ km}$, which is almost the same as $N_{\text{col,cum}}$ at $x = x_c$.

All medium-sized chondrules ($a_{\text{ch,init}} = 10^{2.2} \text{ }\mu\text{m}$) experience collisions with dust particles during melting. These chondrules have larger cross-sections and higher relative velocities to dust particles than the smallest chondrules, which makes the cumulative number of collisions greater. The cumulative number of collisions between chondrules and dust particles exceeds unity during melting, and all chondrules are destroyed.

The largest chondrules ($a_{\text{ch,init}} = 10^3 \text{ }\mu\text{m}$) are not destroyed in collisions. These chondrules do not become droplets, and they can avoid destructive collisions. The chondrules are eroded by collisions between the solid chondrules and the dust. The final size and mass of the chondrules are 96.8% and 90.6% of the initial size and mass. Of the total size change of the chondrules, 90% (corresponding to $0.971a_{\text{ch}}$) occurs up to $x = 210 \text{ km}$, where about 530 out of 1121 collisions occur. The chondrules are mainly eroded by high-velocity collisions, $v_{\text{imp}} > 6 \text{ km s}^{-1}$, in the short distance. The effect of the low-velocity collisions in the long distance on the erosion rate is small.

We find three fates of chondrule (precursors): (1) small collisionless chondrules ($\lesssim 10^2 \text{ }\mu\text{m}$) survive; (2) $10^2 \text{ }\mu\text{m} \lesssim a_{\text{ch,init}} \lesssim 10^3 \text{ }\mu\text{m}$ chondrules are destroyed during melting; and (3) large unmelted chondrules (precursors) ($\gtrsim 10^3 \text{ }\mu\text{m}$) do not melt and survive. The survival of the large unmelted chondrules (precursors) is consistent with Nakamoto & Miura (2004). The survival of the small collisionless chondrule is similar to the compound chondrules formation, where the chondrule-chondrule collisions are rare (Ciesla 2006; Arakawa & Nakamoto 2019). The destruction of the medium-sized chondrules during melting is our key finding.

3.2. Parameter of chondrule destruction

The types of chondrule evolution are characterized by two conditions: melting and collision. We show the final states of the chondrules on the initial chondrule diameter ($d_{\text{ch,init}} = 2a_{\text{ch,init}}$) and the shock velocity (v_0) plane in Figure 3. Large chondrules do not melt at low shock velocities. Some of small chondrules do not experience collisions. Chondrules that satisfy the melting and collision conditions are destroyed during melting. The melting condition is roughly estimated by substituting the melting temperature into the equation of energy (Equation (7)). The collision condition is estimated by

³ This assumption is based on impact studies (e.g., Wünnemann et al. 2010; Bisighini et al. 2010). When the thickness of the molten part is shorter than the dust size, this assumption is not good and the solid part is also ejected. We note that this criterion for the ejection from the lower solid part would change if the molten part contained relict grains (e.g., Hewins et al. 2005; Jacquet et al. 2021). This assumption does not affect our results.

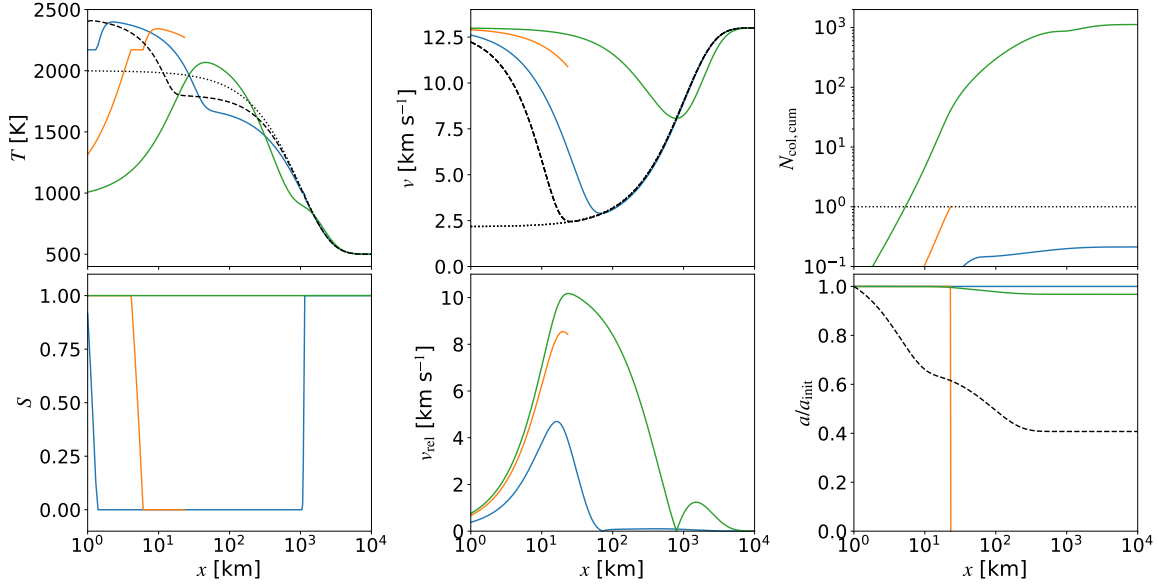


Figure 2. Temperature (T), solid mass fraction (S), velocity with respect to the shock front (v), relative velocity (v_{rel}), cumulative number of collisions ($N_{\text{col,cum}}$), and size ratio to the initial one (a/a_{init}) are plotted against distance from the shock front in the case that $v_0 = 13 \text{ km s}^{-1}$, $\chi = 0.1$, and $a_{\text{d,init}} = 20 \mu\text{m}$. The solid lines are the quantities of the chondrules. The different colors indicate the different initial sizes of the chondrules, $a_{\text{ch,init}} = 10^{1.6} (= 39.8) \mu\text{m}$ (blue), $10^{2.2} (= 158) \mu\text{m}$ (orange), and $10^3 \mu\text{m}$ (green). In the panels of T and v , the dotted lines are those of the gas. In the panels of T , v , and a/a_{init} , the dashed lines are those of the dust particles. The dotted line in the $N_{\text{col,cum}}$ panel is the line for $N_{\text{col,cum}} = 1$.

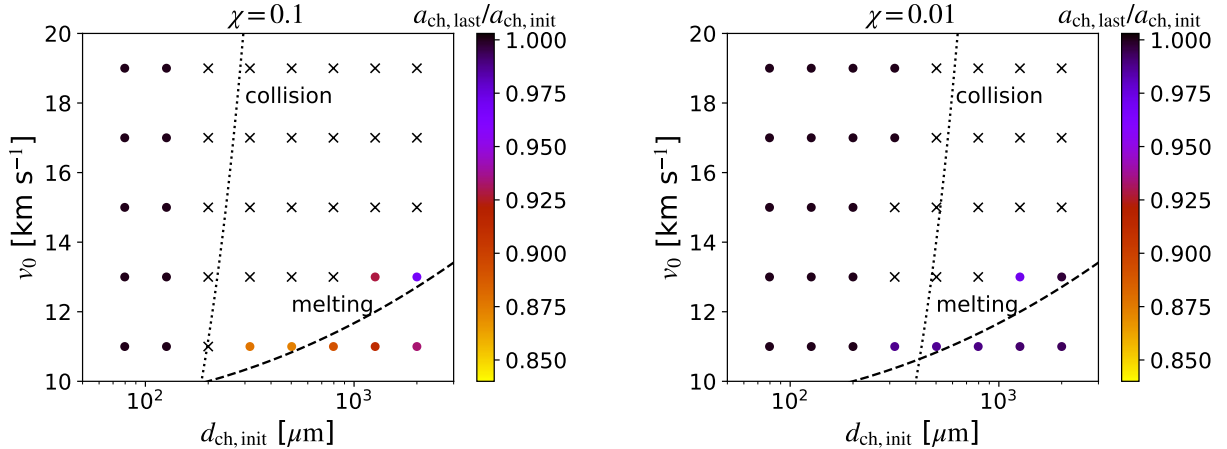


Figure 3. Final states of the chondrules are plotted on the initial chondrular diameter ($d_{\text{ch,init}}$) and the shock velocity (v_0) planes. In the case of the chondrular survival, we plot the circle symbols, whose colors represent the size ratios of the final chondrules to the initial ones. The case of chondrular destruction is represented by the cross symbols. The dotted lines and dashed lines are the collision condition (Equations (13)) and the melting condition. The left and right panels show the cases of $\chi = 0.1$ and $\chi = 0.01$, respectively.

integrating the number of collisions. This integration is approximately given by $n_{\text{col}} l_{\text{stop,ch}}$ for small chondrules. Given that the number density of dust particles is the same as that in the preshock region, the collision condition is expressed as,

$$\Leftrightarrow a_{\text{ch,init}} > 0.9 \times 10^2 \mu\text{m} \left(\frac{v_0}{10 \text{ km s}^{-1}} \right)^{2/3} \times \left(\frac{\chi}{0.1} \right)^{-1/3} \left(\frac{a_{\text{d}}}{20 \mu\text{m}} \right). \quad (13)$$

$$n_{\text{col}} l_{\text{stop,ch}} \sim \left(\chi \frac{m_g n_0}{m_d} \right) \pi a_{\text{ch}}^2 \frac{v_{\text{imp}}}{v_{\text{ch}}} l_{\text{stop,ch}} > 1,$$

This equation approximately reproduces the boundary of the collision in Figure 3.

The final sizes of the unmelted chondrules are comparable to the initial sizes (the bottom right of Figure 3). The ratios of the final sizes to the initial sizes, $a_{\text{ch,last}}/a_{\text{ch,init}}$, are greater than 0.87. These chondrules experience many low-velocity collisions (Section 3.1). These collisions do not cause erosion but would cause accretion (Matsumoto & Arakawa 2023).

Equation (13) shows that the typical size of the observed chondrules, $\sim 10^2\text{--}10^3 \mu\text{m}$ (e.g., Friedrich et al. 2015), satisfies the collision condition. This suggests that the observed chondrules are not formed in the shock heating events when small dust particles coexist. The shock events that form chondrules are different from the shock events that melt and accrete igneous rims.

4. CONCLUSION AND DISCUSSION

Chondrules and igneous rims are considered to experience similar heating events in the solar nebula. We consider the shock wave heating in their (precursors) coexistence. We focus on the destruction of chondrules in collisions with dust particles. We find three regimes: the survival of collisionless chondrules; the destruction of chondrules by collisions during melting; and the survival of unmolten chondrules. The collisionless chon-

drules have an initial size of $\lesssim 10^2 \mu\text{m}$. The chondrules larger than this size are destroyed by collisions if they melt, and they are not destroyed if they do not melt. This suggests that the chondrule-forming shock events are destructive to chondrules in the presence of dust particles and that they are distinct from the rim-accreting shock events.

The key point of this work is the presence of $\sim 10 \mu\text{m}$ dust particles for the destruction of $\sim 1 \text{ mm}$ chondrules. If the dust particles are large and comparable to the size of the chondrules, the destruction of chondrules by collisions during melting does not occur (Ciesla 2006; Arakawa & Nakamoto 2019). If the dust sizes are $\lesssim 1 \mu\text{m}$, the dust is completely evaporated and the chondrule destruction occurs if the molten chondrules experience collisions before the whole dust evaporation (Appendix D).

We thank Prof. A. M. Nakamura for comments on the strength of chondrules. Numerical simulations were in part carried out on analysis servers at Center for Computational Astrophysics, National Astronomical Observatory of Japan.

APPENDIX

A. HEATING AND COOLING RATES OF A PARTICLE

The heating rate via the energy transfer from the gas, Γ , is given by

$$\Gamma = m_g n_g |v - v_g| (T_{\text{rec}} - T) C_H, \quad (\text{A1})$$

where the recovery temperature, T_{rec} , and a heat transfer function, C_H , are (e.g., Gombosi et al. 1986)

$$T_{\text{rec}} = \frac{T_g}{\gamma + 1} \left[2\gamma + 2(\gamma - 1)s^2 - \frac{\gamma - 1}{0.5 + s^2 + (s/\sqrt{\pi}) \exp(-s^2) \text{erf}^{-1}(s)} \right], \quad (\text{A2})$$

and

$$C_H = \frac{\gamma + 1}{\gamma - 1} \frac{k_B}{8m_g s^2} \left[\frac{s}{\sqrt{\pi}} \exp(-s^2) + \left(\frac{1}{2} + s^2 \right) \text{erf}(s) \right], \quad (\text{A3})$$

respectively. The radiative cooling rate is given by

$$\Lambda_{\text{rad}} = \epsilon_{\text{emit}} \sigma_{\text{SB}} T^4 - \epsilon_{\text{emit}} \sigma_{\text{SB}} T_0^4, \quad (\text{A4})$$

where ϵ_{emit} is the emission coefficient and $\sigma_{\text{SB}} = 5.67 \times 10^{-5} \text{ erg cm}^{-2} \text{ K}^{-4} \text{ s}^{-1}$ is the Stefan–Boltzmann constant. The emission coefficient is (Rizk et al. 1991; Miura & Nakamoto 2005)

$$\epsilon_{\text{emit}} = \min \left[2.1543 \times 10^{-3} \left(\frac{a}{1 \mu\text{m}} \right)^{0.8253}, 1 \right]. \quad (\text{A5})$$

The latent heat cooling by evaporation is the product of the evaporation rate, J_{evap} , and the latent heat of evaporation, L_{evap} ,

$$\Lambda_{\text{evap}} = J_{\text{evap}} L_{\text{evap}}, \quad (\text{A6})$$

where J_{evap} is

$$J_{\text{evap}} = 691 \left(\frac{p_{\text{H}_2}}{100 \text{ dyn cm}^{-2}} \right)^{1/2} \left(\frac{T}{T_{\text{melt}}} \right)^{-1/2} \exp \left(-\frac{3.17 \times 10^4 \text{ K}}{T} \right) \text{ g cm}^{-2} \text{ s}^{-1}, \quad (\text{A7})$$

and $L_{\text{evap}} = 1.12 \times 10^{11} \text{ erg g}^{-1}$ for forsterite (Miura et al. 2002). The ambient gas pressure, p_{H_2} , is the summation of the thermal pressure and the ram pressure⁴,

$$p_{\text{H}_2} = n_{\text{g}} k_{\text{B}} T_{\text{g}} + \frac{1}{3} m_{\text{g}} n_{\text{g}} (v - v_{\text{g}})^2. \quad (\text{A8})$$

B. BOILING AND EVAPORATION OF A DUST PARTICLES

Dust particles boil when their vapor pressure, p_{eq} , exceeds the gas pressure, p_{H_2} (Miura et al. 2002, see also Nagahara & Ozawa (1996)), where

$$p_{\text{eq}} = 3.20 \times 10^8 \exp \left(-\frac{6.18 \times 10^4 \text{ K}}{T} \right) \text{ bar}. \quad (\text{B9})$$

The boiling rate of a dust particle is

$$-4\pi a_d^2 \rho_d L_{\text{boil}} \left(\frac{da_d}{dx} \right)_{\text{boil}} = \frac{4\pi a_d^2}{v_d} (\Gamma - \Lambda_{\text{rad}} - \Lambda_{\text{evap}}), \quad (\text{B10})$$

where $L_{\text{boil}} = 1.64 \times 10^{11} \text{ erg g}^{-1}$ is the latent heat of boiling (Miura et al. 2002). The size of a dust particle also decreases due to evaporation from the precursor surface, and its rate is

$$-4\pi a_d^2 \rho_d \left(\frac{da_d}{dx} \right)_{\text{evap}} = \frac{4\pi a_d^2}{v_d} J_{\text{evap}}. \quad (\text{B11})$$

C. BREAKUP CRITERIA OF DROPLET COLLISIONS

The breakup criteria of droplets in collisions are characterized by the Weber number, We ,

$$We = \frac{2\rho a v_{\text{imp}}^2}{\sigma}, \quad (\text{C12})$$

where σ is the surface tension. A droplet is destroyed when We exceeds the critical value, We_{cr} . It is known that $We_{\text{cr}} \sim 10$ for the droplet-flow interaction (e.g., Bronshten 1983; Kadono & Arakawa 2005; Kadono et al. 2008). Substituting $We_{\text{cr}} \sim 10$ and $\sigma = 400 \text{ erg cm}^{-2}$ (Murase & McBirney 1973), we can get the critical velocity,

$$v_{\text{cr}} \sim 100 \text{ cm s}^{-1} \left(\frac{a_{\text{ch}}}{0.1 \text{ cm}} \right)^{-1/2} \left(\frac{We_{\text{cr}}}{10} \right)^{1/2}. \quad (\text{C13})$$

The criterion for the collisional destruction of the droplets is different from this droplet-flow interaction criterion. The collision experiments of the droplets show that the outcomes of the droplets with $We \gtrsim 10$ are coalescence, bounce, and separation according to the Weber number and impact parameters (e.g., Qian & Law 1997, see also Ciesla (2006)). There are some experimental and numerical studies considering collisions of droplets with We higher than ~ 10 . Pan et al. (2009) performed experiments on head-on collisions of equal-sized droplets at high Weber numbers and showed that droplet collisions become destructive when

$$We \geq 301.0 + 1124.3 \mathcal{O}h, \quad (\text{C14})$$

where the Ohnesorge number, $\mathcal{O}h$, is given the ratio between the viscous and surface energies,

$$\mathcal{O}h = \frac{\eta}{\sqrt{2\rho\sigma a}}, \quad (\text{C15})$$

⁴ The pressure of the net gas-grain flow on the product of the evaporation rate is unclear and not included in this study.

and η is the viscosity. Substituting the viscosity of the chondrules in H3 chondrites (Hubbard 2015),

$$\log_{10} \left(\frac{\eta}{1 \text{ P}} \right) = -3.55 + \frac{5084.9 \text{ K}}{T - 584.9 \text{ K}}, \quad (\text{C16})$$

the Ohnesorge number of a chondrule becomes

$$\mathcal{O}h = 6.5 \times 10^{-5.55 + \frac{5084.9 \text{ K}}{T_{\text{ch}} - 584.9 \text{ K}}} \left(\frac{\rho_{\text{ch}}}{3 \text{ g cm}^{-3}} \right)^{-1/2} \left(\frac{\sigma}{400 \text{ erg cm}^{-2}} \right)^{-1/2} \left(\frac{a_{\text{ch}}}{0.1 \text{ cm}} \right)^{-1/2}. \quad (\text{C17})$$

The critical Weber number begins to increase rapidly due to the contribution of the Ohnesorge number when the temperature becomes less than about 1800 K. In this case, we can rewrite the critical velocity as,

$$v_{\text{cr}} \sim 5 \text{ cm s}^{-1} \times 10^{\frac{2542.5 \text{ K}}{T_{\text{ch}} - 584.9 \text{ K}}} \left(\frac{\rho_{\text{ch}}}{3 \text{ g cm}^{-3}} \right)^{-1/4} \left(\frac{\sigma}{400 \text{ erg cm}^{-2}} \right)^{-1/4} \left(\frac{a_{\text{ch}}}{0.1 \text{ cm}} \right)^{-3/4}. \quad (\text{C18})$$

We consider that the critical velocity of droplet destruction in collisions is much lower than $\sim 1 \text{ km s}^{-1}$, and we assume that the collisions between the droplet chondrules and droplet dust particles are destructive in the postshock region. We note that supercooled droplets with extremely high viscosity are expected to survive high-velocity collisions (Arakawa & Nakamoto 2019; Matsumoto & Arakawa 2023), but the survival of supercooled droplets does not significantly change the results of this paper. This is because the critical velocity for droplet destruction becomes 1 km s^{-1} when T becomes less than $\sim 1200 \text{ K}$.

D. EFFECT OF DUST EVAPORATION

In the case of $a_d = 20 \mu\text{m}$ and $n_0 = 10^{14} \text{ cm}^{-3}$, dust particles are completely evaporated when $v_0 \geq 17 \text{ km s}^{-1}$. When $v_0 = 17 \text{ km s}^{-1}$, the complete dust evaporation occurs at $x \simeq 2.1 \times 10^2 \text{ km}$. In this case, molten chondrules can avoid destructive collisions when $a_{\text{ch}} \gtrsim 5 \text{ mm}$. Chondrules with $a_{\text{ch}} \lesssim 5 \text{ mm}$ are destroyed by collisions. This is because they melt at $x < 2.1 \times 10^2 \text{ km}$ and the molten chondrules collide with the dust particles before complete evaporation.

The effect of the dust evaporation can help $\sim 1 \text{ mm}$ chondrules to survive in the shock wave when the dust size is $\lesssim 1 \mu\text{m}$. Figure 4 shows the final states of the chondrules in the case of $a_d = 2 \mu\text{m}$ and $\chi = 0.1$, where the critical velocity for the dust evaporation is less than 10 km s^{-1} . Since the dust particles are evaporated, there are some parameters, in which $\sim 1 \text{ mm}$ chondrules can survive although they are molten. This suggests that the presence of the $\lesssim 1 \mu\text{m}$ dust particles does not prevent chondrules from forming in shock waves.

REFERENCES

- Arakawa, S., & Nakamoto, T. 2016, *Icarus*, 276, 102, doi: [10.1016/j.icarus.2016.04.041](https://doi.org/10.1016/j.icarus.2016.04.041)
- . 2019, *ApJ*, 877, 84, doi: [10.3847/1538-4357/ab1b3e](https://doi.org/10.3847/1538-4357/ab1b3e)
- Ashworth, J. R. 1977, *Earth and Planetary Science Letters*, 35, 25, doi: [10.1016/0012-821X\(77\)90024-3](https://doi.org/10.1016/0012-821X(77)90024-3)
- Asphaug, E., Jutzi, M., & Movshovitz, N. 2011, *Earth and Planetary Science Letters*, 308, 369, doi: [10.1016/j.epsl.2011.06.007](https://doi.org/10.1016/j.epsl.2011.06.007)
- Bisighini, A., Cossali, G. E., Tropea, C., & Roisman, I. V. 2010, *PhRvE*, 82, 036319, doi: [10.1103/PhysRevE.82.036319](https://doi.org/10.1103/PhysRevE.82.036319)
- Bronshten, V. A. 1983, *Physics of Meteoric Phenomena*
- Ciesla, F. J. 2006, *M&PS*, 41, 1347, doi: [10.1111/j.1945-5100.2006.tb00526.x](https://doi.org/10.1111/j.1945-5100.2006.tb00526.x)
- Friedrich, J. M., Weisberg, M. K., Ebel, D. S., et al. 2015, *Chemie der Erde / Geochemistry*, 75, 419, doi: [10.1016/j.chemer.2014.08.003](https://doi.org/10.1016/j.chemer.2014.08.003)
- Gombosi, T. I., Nagy, A. F., & Cravens, T. E. 1986, *Reviews of Geophysics*, 24, 667, doi: [10.1029/RG024i003p00667](https://doi.org/10.1029/RG024i003p00667)
- Hewins, R. H., Connolly, H. C., Lofgren, G. E., J., & Libourel, G. 2005, in *Astronomical Society of the Pacific Conference Series*, Vol. 341, *Chondrites and the Protoplanetary Disk*, ed. A. N. Krot, E. R. D. Scott, & B. Reipurth, 286
- Holsapple, K. A. 1993, *Annual Review of Earth and Planetary Sciences*, 21, 333, doi: [10.1146/annurev.ea.21.050193.002001](https://doi.org/10.1146/annurev.ea.21.050193.002001)
- Holsapple, K. A., & Schmidt, R. M. 1982, *J. Geophys. Res.*, 87, 1849, doi: [10.1029/JB087iB03p01849](https://doi.org/10.1029/JB087iB03p01849)

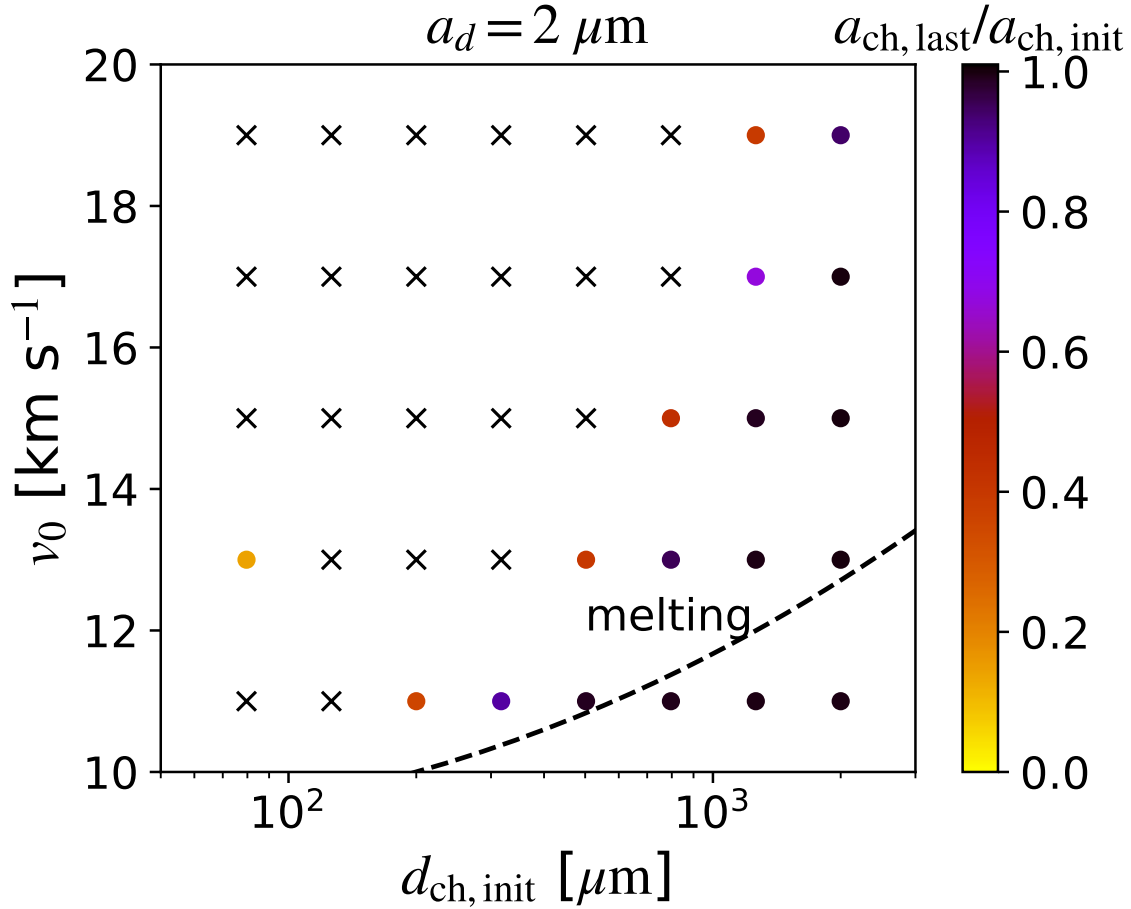


Figure 4. Same as Figure 3, but for the case of $a_d = 2 \mu\text{m}$ and $\chi = 0.1$. The minimum size for collisional destruction is $a_{\text{ch, init}} = 9 \mu\text{m}$

(Equations (13)) and is satisfied in all cases.

- Hood, L. L., & Horanyi, M. 1991, *Icarus*, 93, 259, doi: [10.1016/0019-1035\(91\)90211-B](https://doi.org/10.1016/0019-1035(91)90211-B)
- Horányi, M., Morfill, G., Goertz, C. K., & Levy, E. H. 1995, *Icarus*, 114, 174, doi: [10.1006/icar.1995.1052](https://doi.org/10.1006/icar.1995.1052)
- Hubbard, A. 2015, *Icarus*, 254, 56, doi: [10.1016/j.icarus.2015.02.030](https://doi.org/10.1016/j.icarus.2015.02.030)
- Huss, G. R., Alexander, C. M. O., Palme, H., Bland, P. A., & Wasson, J. T. 2005, in *Astronomical Society of the Pacific Conference Series*, Vol. 341, *Chondrites and the Protoplanetary Disk*, ed. A. N. Krot, E. R. D. Scott, & B. Reipurth, 701
- Iida, A., Nakamoto, T., Susa, H., & Nakagawa, Y. 2001, *Icarus*, 153, 430, doi: [10.1006/icar.2001.6682](https://doi.org/10.1006/icar.2001.6682)
- Jacquet, E., Paulhiac-Pison, M., Alard, O., Kearsley, A. T., & Gounelle, M. 2013, *M&PS*, 48, 1981, doi: [10.1111/maps.12212](https://doi.org/10.1111/maps.12212)
- Jacquet, E., Piralla, M., Kersaho, P., & Marrocchi, Y. 2021, *M&PS*, 56, 13, doi: [10.1111/maps.13583](https://doi.org/10.1111/maps.13583)
- Jacquet, E., & Thompson, C. 2014, *ApJ*, 797, 30, doi: [10.1088/0004-637X/797/1/30](https://doi.org/10.1088/0004-637X/797/1/30)
- Johnson, B. C., Minton, D. A., Melosh, H. J., & Zuber, M. T. 2015, *Nature*, 517, 339, doi: [10.1038/nature14105](https://doi.org/10.1038/nature14105)
- Kadono, T., & Arakawa, M. 2005, *Icarus*, 173, 295, doi: [10.1016/j.icarus.2004.08.014](https://doi.org/10.1016/j.icarus.2004.08.014)
- Kadono, T., Arakawa, M., & Kouchi, A. 2008, *Icarus*, 197, 621, doi: [10.1016/j.icarus.2008.05.002](https://doi.org/10.1016/j.icarus.2008.05.002)
- Kaneko, H., Arakawa, S., & Nakamoto, T. 2022, *Icarus*, 374, 114726, doi: [10.1016/j.icarus.2021.114726](https://doi.org/10.1016/j.icarus.2021.114726)
- Kaneko, H., Sato, K., Ikeda, C., & Nakamoto, T. 2023, *ApJ*, 947, 15, doi: [10.3847/1538-4357/acb20e](https://doi.org/10.3847/1538-4357/acb20e)
- Kring, D. A. 1991, *Earth and Planetary Science Letters*, 105, 65, doi: [10.1016/0012-821X\(91\)90121-W](https://doi.org/10.1016/0012-821X(91)90121-W)
- Krot, A. N., & Wasson, J. T. 1995, *Geochimica et Cosmochimica Acta*, 59, 4951, doi: [10.1016/0016-7037\(95\)00337-1](https://doi.org/10.1016/0016-7037(95)00337-1)
- Matsumoto, Y., & Arakawa, S. 2023, *ApJ*, 948, 73, doi: [10.3847/1538-4357/acc57c](https://doi.org/10.3847/1538-4357/acc57c)

- Matsumoto, Y., Hasegawa, Y., Matsuda, N., & Liu, M.-C. 2021, *Icarus*, 367, 114538, doi: [10.1016/j.icarus.2021.114538](https://doi.org/10.1016/j.icarus.2021.114538)
- Matsumoto, Y., Wakita, S., Hasegawa, Y., & Oshino, S. 2019, *The Astrophysical Journal*, 887, 248, doi: [10.3847/1538-4357/ab5b06](https://doi.org/10.3847/1538-4357/ab5b06)
- Metzler, K., Bischoff, A., & Stoeffler, D. 1992, *Geochimica et Cosmochimica Acta*, 56, 2873, doi: [10.1016/0016-7037\(92\)90365-P](https://doi.org/10.1016/0016-7037(92)90365-P)
- Miura, H., & Nakamoto, T. 2005, *Icarus*, 175, 289, doi: [10.1016/j.icarus.2004.11.011](https://doi.org/10.1016/j.icarus.2004.11.011)
- Miura, H., Nakamoto, T., & Susa, H. 2002, *Icarus*, 160, 258, doi: [10.1006/icar.2002.6964](https://doi.org/10.1006/icar.2002.6964)
- Murase, T., & McBirney, A. R. 1973, *Geological Society of America Bulletin*, 84, 3563, doi: [10.1130/0016-7606\(1973\)84<3563:POSCIR>2.0.CO;2](https://doi.org/10.1130/0016-7606(1973)84<3563:POSCIR>2.0.CO;2)
- Nagahara, H., & Ozawa, K. 1996, *GeoCoA*, 60, 1445, doi: [10.1016/0016-7037\(96\)00014-2](https://doi.org/10.1016/0016-7037(96)00014-2)
- Nagashima, K., Moriuchi, Y., Tsukamoto, K., Tanaka, K. K., & Kobatake, H. 2008, *Journal of Mineralogical and Petrological Sciences*, 103, 204, doi: [10.2465/jmps.070620c](https://doi.org/10.2465/jmps.070620c)
- Nakamoto, T., & Miura, H. 2004, in *Lunar and Planetary Science Conference*, ed. S. Mackwell & E. Stansbery, Lunar and Planetary Science Conference, 1847
- Pan, K.-L., Chou, P.-C., & Tseng, Y.-J. 2009, *PhRvE*, 80, 036301, doi: [10.1103/PhysRevE.80.036301](https://doi.org/10.1103/PhysRevE.80.036301)
- Qian, J., & Law, C. K. 1997, *Journal of Fluid Mechanics*, 331, 59, doi: [10.1017/S0022112096003722](https://doi.org/10.1017/S0022112096003722)
- Rizk, B., Hunten, D. M., & Engel, S. 1991, *J. Geophys. Res.*, 96, 1303, doi: [10.1029/90JA01998](https://doi.org/10.1029/90JA01998)
- Rubin, A. E. 1984, *Geochimica et Cosmochimica Acta*, 48, 1779, doi: [10.1016/0016-7037\(84\)90032-2](https://doi.org/10.1016/0016-7037(84)90032-2)
- . 2010, *Geochimica et Cosmochimica Acta*, 74, 4807, doi: [10.1016/j.gca.2010.05.018](https://doi.org/10.1016/j.gca.2010.05.018)
- Scott, E. R. D. 2007, *Annual Review of Earth and Planetary Sciences*, 35, 577, doi: [10.1146/annurev.earth.35.031306.140100](https://doi.org/10.1146/annurev.earth.35.031306.140100)
- Suzuki, A., Hakura, S., Hamura, T., et al. 2012, *Journal of Geophysical Research (Planets)*, 117, E08012, doi: [10.1029/2012JE004064](https://doi.org/10.1029/2012JE004064)
- Takagi, Y., Mizutani, H., & Kawakami, S.-I. 1984, *Icarus*, 59, 462, doi: [10.1016/0019-1035\(84\)90114-3](https://doi.org/10.1016/0019-1035(84)90114-3)
- Villeneuve, J., Libourel, G., & Soulié, C. 2015, *GeoCoA*, 160, 277, doi: [10.1016/j.gca.2015.03.033](https://doi.org/10.1016/j.gca.2015.03.033)
- Wada, K., Grott, M., Michel, P., et al. 2018, *Progress in Earth and Planetary Science*, 5, 82, doi: [10.1186/s40645-018-0237-y](https://doi.org/10.1186/s40645-018-0237-y)
- Wakita, S., Matsumoto, Y., Oshino, S., & Hasegawa, Y. 2017, *ApJ*, 834, 125, doi: [10.3847/1538-4357/834/2/125](https://doi.org/10.3847/1538-4357/834/2/125)
- Wünnemann, K., Collins, G. S., & Weiss, R. 2010, *Reviews of Geophysics*, 48, RG4006, doi: [10.1029/2009RG000308](https://doi.org/10.1029/2009RG000308)